Finite Element Analysis of a vehicle chassis cross-member spot weld design

RMRC Udayanandana[1#], PPSS Pussepitiya[2] and Jens Lahr[3]

[1] *Department of Mechanical Engineering, Advanced technological Institute,Colombo 15, Sri Lanka*
[2]*Department of Aeronautical Engineering, Faculty of Engineering, General Sir John Kotelawala Defence University, Sri Lanka.*
[3]*Faculty of Computing, Engineering and Built Environment, Birmingham City University, United Kingdom*
[#] udayanandana@gmail.com

Abstract*—*This paper addresses the analysis of LDV light commercial van chassis cross member spot weld design. First the experimental test was conducted to measure the deflection and strain values under different load conditions. A linear elastic finite element analysis was done on the beam to obtain predictions of deflections and strains at strain gauge locations and compare with measured values and the finite element predictions was analysed through the manual calculations based on Mechanics of Materials. The structure was modelled with two main solid parts and spot welded together and the spot welds were modelled by using point icon through Ansys 14 software. The main part and model generated by using Solidworks software during the study. The results were compared and validated to develop a suitable FEA model for design change analysis. Finally an efficient and cost effective design was proposed.

Keywords: spot weld, FEA model and cost effective design

I. INTRODUCTION

Spot welding is a widely used method for manufacturing of thin-sheet components, especially in mass-production industries such as the automotive industry. Optimization of the number and location of the spot welds under fatigue conditions is a major economic consideration. Because of mass production, a small reduction of the number of spot welds, through their efficient and optimal usage, can mean a great saving in production cost. Every vehicle has a body, which has to carry both the loads and its own weight. Vehicle body consists of two parts; chassis and bodywork or superstructure. The conventional chassis frame, which is made of pressed steel members, is considered in this research.

The main advantage ofthis approach is the simplicityof the bar model of spot welds and a relatively simple finite element (FE) model of the structure, therefore the optimization analysis is usually not very complex and time consuming. The aim of this research is to investigate the efficiency of the design, particularly the arrangement of spot welds by carrying out a finite element analysis of the chassis member and improve the design. One objective of the research is to conduct a linear elastic finite element analysis of the beam to obtain predictions of deflections and strains, (at strain gauge locations) and compare with measured values. Another objective is to validate the finite element predictions through manual calculations based on Mechanics of Materials and to determine the optimum model shape and frequencies of the cross-member for on-vehicle conditions.

The commercial finite element package, ANSYS version 14 is used for the solution of the problem and the general arrangement of the chassis frame model is considered as seel bar.

Two of the major problems of any welding process are residual stress and distortion. Welding processes usually result in residual stresses, which are locked in the structural material or component. The effect of the stresses can be either beneficial or detrimental, depending upon their magnitude, sign (tensile or compressive), and distribution with respect to the service induced stresses (Sariel et al, 2006). It has been reported that residual stresses may cause brittle fracture, crack propagation, fatigue life reduction and stress corrosion cracking (Parmar, 1999)

Thus, it is essential to be able to determine the residual stresses, and consider them as a part of the service loads. There are two common methods including: X-ray diffraction and hole-drilling to measure residual stresses within the welded materials (Nodeh, 2007).

II. METHODOLOGY

Experimental tests were carryout in order to obtain the deflection of beam and the strains for different loading conditions.

A. Experiment test

The experiment setup is shown in Figure 1. A dial gauge was used to measure the deflection of the beam. Two strain gauges bonded on top and bottom of the beam was wired to the Strain Indicator devices with quarter bridge strain gauge circuit (Figure 2). A gauge factor of 2.065 was used.

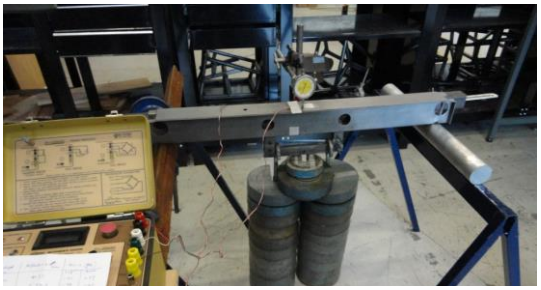

Figure 1: Experimental setup for measuring strains and deflections

Table 1 shows the measured values of strains and deflection for various loading conditions.

Table 1: Strains and deflections for various load values

Mass/(kg)	Deflection/(mm)	Strain /(με)	
		Top	Bottom
40.2	0.10	-31	37
50.2	0.13	-39	46
60.2	0.13	-47	55
70.2	0.15	-54	64
80.2	0.17	-62	73
97.2	0.21	-76	89
101.2	0.22	-79	92

B. Manual calculations

The manual calculation was done considering the approximated cross section of cross member shown in Figure 2. It was separated into three rectangular sections. The calculated cross section values are shown in Table 2.

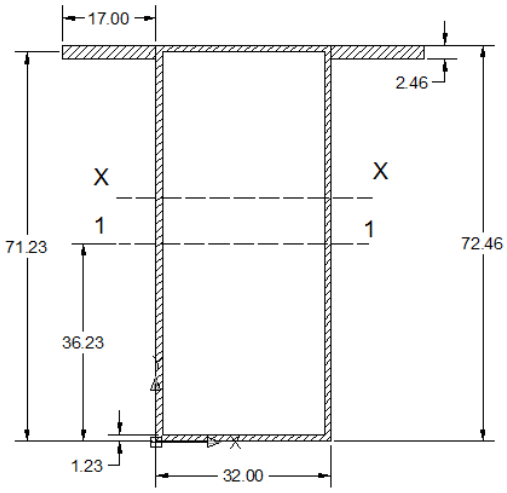

Figure *2:* Approximated cross section of cross member, units are in millimetres

Moment of inertia calculations are shown in Table 2.

Table 2: Moment of inertia calculations

Cross section	Area(A) /(mm^2)	$\bar{y}$ /(mm)	$\bar{y}A$ /(mm^3)
1	250.92	36.23	9090.83
2	41.82	71.23	2978.84
3	41.82	71.23	2978.84
Total	334.56		15048.51

$$\bar{Y} = \frac{\Sigma \bar{y} A}{\Sigma A} = 44.98\ mm$$

Moment of inertia about centroid of cross section,

$$I_x = \Sigma(I + Ad^2)$$

$$= 291888\ mm^4$$

The manual calculations for the total load of 101.2 kg (Table 1) are shown below. The cross member beam is assumed to be simply supported and with uniform cross section,

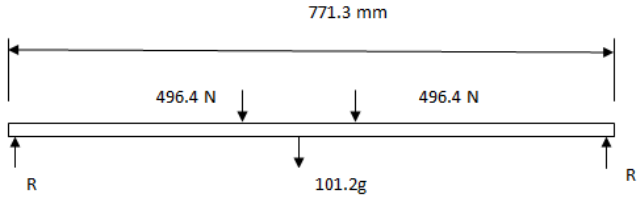

Figure3: simplified cross member with boundary conditions

$$R = 506.3\ N$$

Bending moment at mid point,

$$M = 134.4\ Nm$$

Maximum bending stress at bottom for total 992.8 N load,

$$\sigma = \frac{My}{I} = 20.7\ MPa$$

Strain at bottom,

$$\varepsilon = \frac{\sigma}{E} == 100\ \mu\varepsilon$$

C. Finite Element Analysis

The simplified geometry created in Ansys 14 is shown in Figure 4.

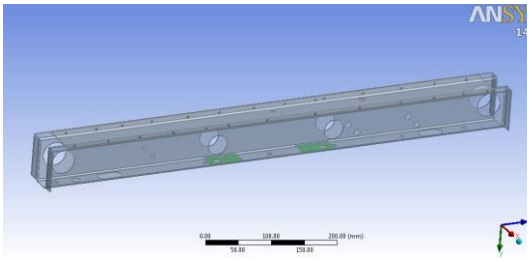

Figure 4: FEA geometry model

The structure consists of two main solid parts spot welded together. The spot welds were modelled by using point icon in Ansys 14. The locations of spot weld points were similar to the real model (Figure 5). As shown in Figure 6, twenty seven weld points were created.

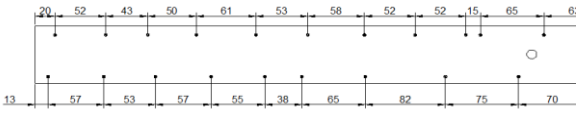

Figure 5: Spot weld positions of existing design

Figure 6: Spot welds modeled in Ansys Workbench 14

Imprint surfaces were created to represent the solid block in the real model for loading, the strain gauges and supporting edges. The loading block was 55 mm x 29 mm and strain gauge was 4 mm x 8 mm in size.

D. Boundary conditions

Remote displacement with freedom to rotate about X axis and motion in Z direction was added to the model. The remote force was applied on to the imprint face in the Y direction (Table 3 and Figure 7).

Table 3: The boundary conditions

Boundary Condition	Position	Value	Direction	Rotation
Remote force	A	496.4 N	Y	-
	B	496.4 N	Y	-
Remote Displacement	C	-	Z	X
	D	-	Z	X

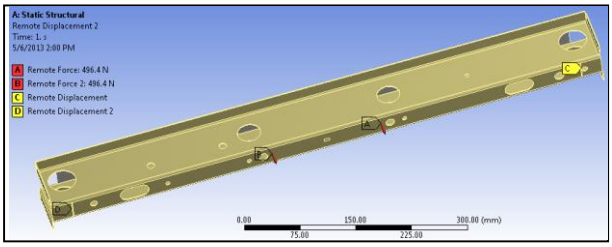

Figure 7: Boundary conditions applied on the FEA model

The behaviour of load acting surface was changed to 'rigid' (Table 4) because of higher thickness solid block was used in real model.The contact between the top plate and bottom structure was changed to frictionless.

Table 4: Applied force on one side

Definition	
Type	Remote Force
Define By	Components
X Component	0. N (ramped)
Y Component	496.4 N (ramped)
Z Component	0. N (ramped)
Suppressed	No
Behavior	Rigid

E. Evaluation of results with mesh refinement

1) Coarse mesh

The generated mesh with default coarse mesh is shown in Figure 8. The quality of the mesh can be accepted when the maximum value of skewness is less than 0.95 (Lee, 2011). The results for top and bottom strains and deformations considered.

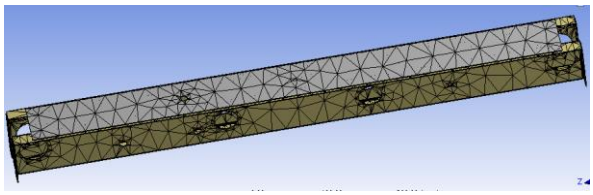

Figure 8: Default coarse mesh

2) Fine mesh

Element mid side node changed from 'program control' to 'kept' to generate parabolic elements (Table 5) and resulted mesh is shown in Figure 9.The area of interest was two strain gauges and the maximum deflection point at the top. So that body sizing with sphere of influence was modelled to refine the mesh in selected area.The resultant mesh is shown in Figure 11. The top strain, bottom strain and top deformation were considered respectively.

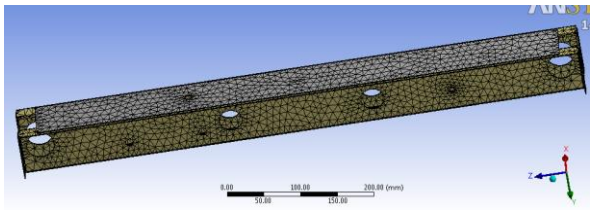

Figure 9: Default fine mesh

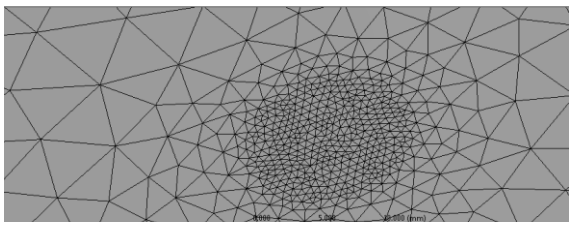

Figure 10: Body sizing with 3mm mesh

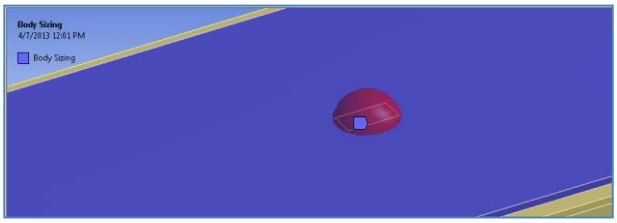

Figure 11: Sphere of influence body sizing

The generated fine mesh with sphere of influence body sizing, the area of interest was two strain gauges and the maximum deflection point at the top. So that body sizing with sphere of influence was modelled to refine the mesh in selected area.The resultant mesh and mesh statistics for 8 mm fine mesh with 0.615 mm mesh sphere of influence body sizing were analysed. The resultant strains and deflection values are shown in Figure 12, Figure 13 and Figure 14 respectively.

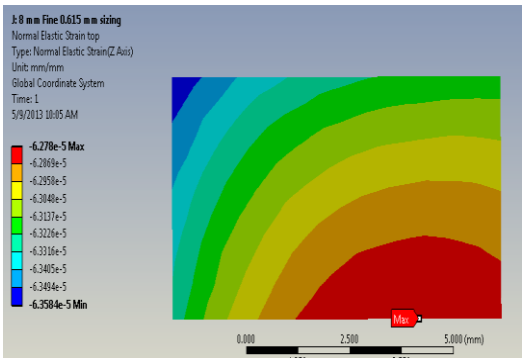

Figure 12: normal elastic strain on top for 8 mm fine mesh with 0.615 mm body sizing

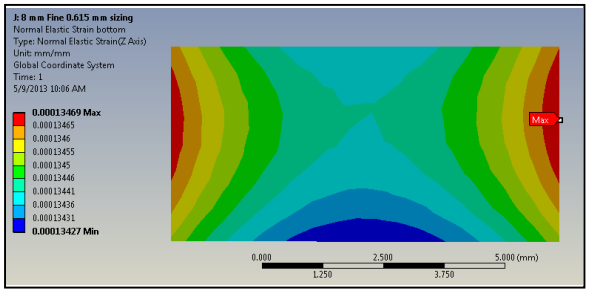

Figure 13: Normal elastic strain at bottom for 8 mm fine mesh with 0.615 mm body sizing

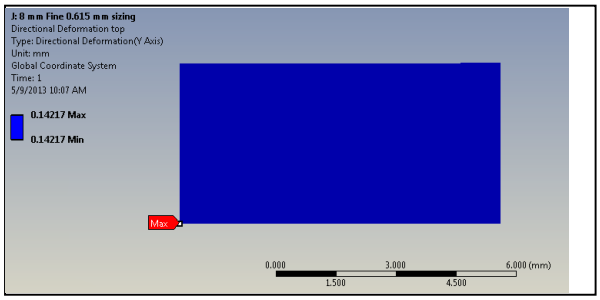

Figure 14: Directional deformation on top for 8 mm fine mesh with 0.615 mm body sizing

IV. RESULTS

The Table 5 shows the results of FEA analysis for different mesh sizes and Figure 15 shows the convergence of deflection with the refinement of mesh.

Table 5: Variation of stress strain and deflection with mesh size for 992.8 N load.

No	Body mesh type	Sphere of influence mesh size (mm)	Number of elements	Strain Top	Strain bottom	Deflection (mm)
1	Coase(40 mm)	-	10909	-53	132	0.113
2	Medium(20 mm)	-	17143	-58	132	0.129
3	Fine (14 mm)	-	29915	-60	134	0.137
4	Fine (14 mm)	3.000	30281	-62	134	0.137
5	Fine (14 mm)	2.000	30834	-61	133	0.137
6	Fine (14 mm)	1.000	33322	-61	134	0.137
7	Fine (14 mm)	0.615	41442	-62	134	0.138
8	Fine (10 mm)	0.615	45730	-63	134	0.139
9	Fine (8 mm)	0.615	59725	-63	134	0.142

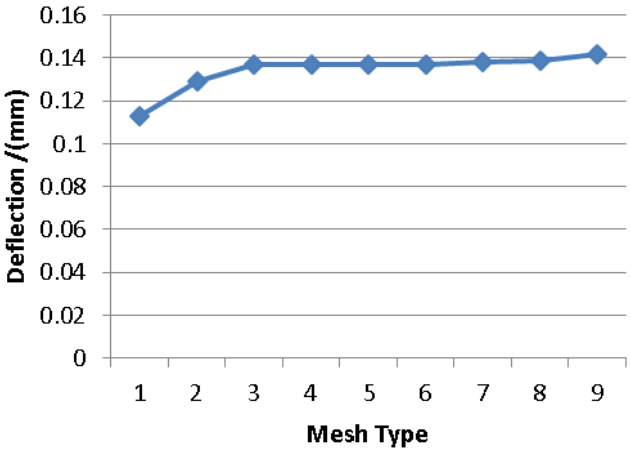

Figure 15: Variation of deflection with mesh size

Table 6: Comparison of experimental, manual calculations and FEA results

	Experimental	Hand Calculation	FEA
Strain-Top/(με)	-79	-61	-63
Strain-Bottom/(με)	92	100	134
Deflection /(mm)	0.22	0.12	0.14

IV. DISCUSSION

By considering the FEA results in Table 5, the top strain and bottom strain have almost converged to -63 με and 134 με respectively. The deflection also converged with 2.1% error. This is a negligible value when compared with the 0.01 mm least count of dial gauge and deflection can be considered as 0.14 mm.

Even though the mesh quality is not good after several refinements, the results can be accepted by considering the convergence. According to Table 6, the FEA model results for the strains and deflections are closer and higher than the manual calculation values. This was due to

assumption of regular cross section made in manual calculations. Actual beam consists of holes on it and deflection should be higher in actual model. But the experimental strain at bottom is less than the hand calculation values. The deflection of experimental value is 57% higher than the FEA model deflection. This could be due to instrumental error or irregularities of thickness and material properties of actual beam.

Typically, a 4-cylinder engine will operate normally between 700 RPM and about 6,000 RPM. Otherwise the vehicle will vibrate between 12 Hz and 100 Hz. According to mode frequencies in Table 7 the structure could reach resonance frequency at 0.26615 Hz and 111.03 Hz. So that the cross member is in safe range of vibration.

The Figure 16 shows the equivalent stress on top plate of the existing cross member. The maximum stress was around the hole. Other green and yellow colour high stress areas were due to tension between weld points and blue colour dots were spot weld points. The Figure 18 shows the proposed pattern for spot welds. The corresponding results for Equivalent stress and linear buckling results are shown in Figure 19 and Figure 20 respectively.

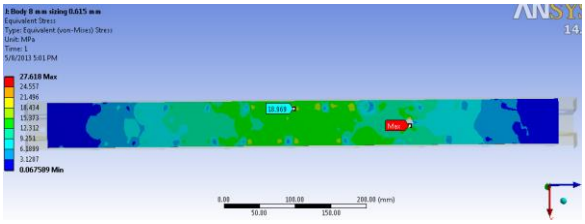

Figure 16:Equivalent stress on top plate of existing design

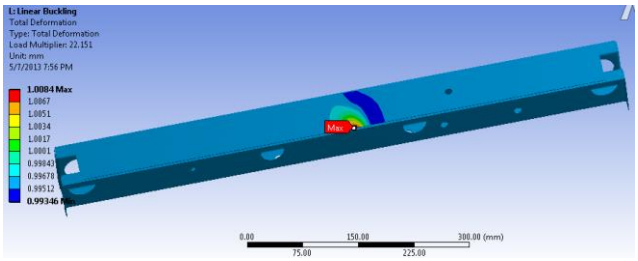

Figure 17: Mode 1 linear buckling for 8 mm fine mesh

Table 7: Frequency values for different mode shapes

Mode	Frequency [Hz]
1.	0.26615
2.	111.03
3.	316.73
4.	416.49
5.	422.49
6.	668.

By considering the equivalent stresses and buckling behaviour, the weld points can be arranged to minimize the stresses.

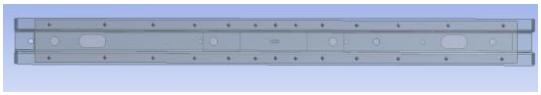

Figure 18: design change with new spot weld positions

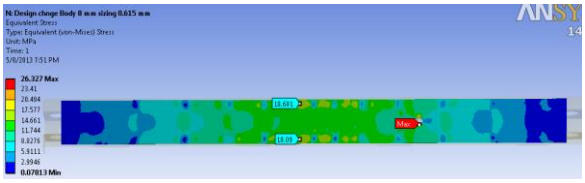

Figure 19: Equivalent stresses of new design

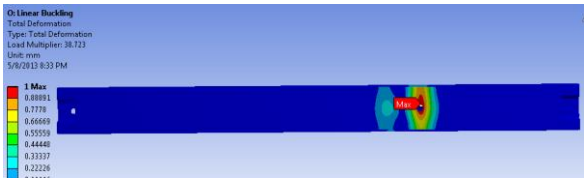

Figure20: linear buckling behaviour of new design

Table 8: Comparison of existing and proposed designs

Property	Existing Design	Proposed Design
Load applied/(N)	992.8	992.8
No of weld points	27	26
Maximum Equivalent Stress/ (M Pa)	27.618	26.327
Total load required to buckle/ (kN)	22.0	38.4

V. CONCLUSIONS

The paper has focused the attention on the experimental and numerical study of the chassis cross member

An application of the verification and validation methodology has been presented to assess the capability of finite element models to predict the optimum spot welding pattern and natural frequencies

Based on the results of this evaluation, the following observations and conclusions can be made.

1. Successful linear elastic finite element model was developed to obtain predictions of deflections and strains
2. The finite element model was validated by considering the convergence of the results, experimental and theoretical calculations.
3. The proposed pattern for the spot weld has 26 weld points which is one weld point less than the

original design and increase in strength of chassis cross member (Table 8)

REFERENCES

1. *Ansys workbench,* software, version 14, ANSYS, Inc.,USA.
2. Lee, H. H., 2011. *Finite element simulations with Ansys Workbench 13 theory-applications-case studies.* Mission: Schroffdevelopment corporation.
3. Martinson, P. et al, 2009. Residual stress analysis of laser spot welding of steel sheets.
4. Nodeh, R., Serajzadeh, S. and Kokabi, A.H. 2008.Simulation of welding residual stresses in resistance spot welding, FE modeling and X-ray verification.
5. Parmar, R.S., 1999. Welding Processes and Technology, second ed.Khanna Publishers, New Delhi.
6. Sariel J et al, 2006,Residual stress distributions in GTA spot welded Ti6Al4V disks, JCPDS-International Centre for Diffraction Data 2006 ISSN 1097-0002.